


Article

The Intrapelvic Pressure during Retrograde Intrarenal Surgery in the Setting of Ureteral Access Sheath Size: Experimental Study on 3D Printed Model

Krzysztof Balawender ^{1,2,*} , Anna Pliszka ¹ and Mariusz Oleksy ³

¹ Department of Normal and Clinical Anatomy, Institute of Medical Sciences, Medical College, Rzeszow University, ul. Leszka Czarnego 4, 35-615 Rzeszów, Poland; annapliszka96@gmail.com

² Clinical Department of Urology and Urological Oncology, Municipal Hospital in Rzeszow, ul. Rycerska 4, 35-241 Rzeszów, Poland

³ Department of Polymer Composites, Faculty of Chemistry, Rzeszow University of Technology, al. Powstańców Warszawy 6, 35-959 Rzeszów, Poland; molek@prz.edu.pl

* Correspondence: balawender82@gmail.com

Abstract: **Introduction:** There is no standardised, universal method to assess physical conditions such as pressure in the pelvicalyceal system in real time during RIRS (retrograde intrarenal surgery). Therefore, the problem of increased pressure in the upper urinary tract during the procedure is underestimated. Moreover, it can potentially cause micro-damage and longer postoperative recovery. The aim of this study was to evaluate intrapelvic pressure (IPP) during RIRS procedures. **Materials and Methods:** The 3D printed models of the pelvicalyceal system were printed based on a CT scan of the real patient. They were used to perform 50 RIRS procedures with laser lithotripsy of artificially synthesised kidney stones with two different sizes of ureteral access sheath-UAS (10/12Fr vs. 12/14Fr) together with different energy settings generated by the holmium:YAG laser. IPP monitoring during RIRS was performed with the use of the PressureWire X Guidewire compatible with the CoroFlow system. **Results and Conclusions:** The results showed that a high IPP of up to 400 cmH₂O would be achieved using a 10/12Fr UAS, while the use of a 12/14Fr UAS would significantly reduce the peak pressure to approximately 100 cmH₂O; hence, the size of the UAS is a pivotal factor of the IPP generated during the procedure.

Keywords: retrograde intrarenal surgery; intrapelvic pressure; 3D printing; ureteral access sheath



Citation: Balawender, K.; Pliszka, A.; Oleksy, M. The Intrapelvic Pressure during Retrograde Intrarenal Surgery in the Setting of Ureteral Access Sheath Size: Experimental Study on 3D Printed Model. *Appl. Sci.* **2023**, *13*, 12385. <https://doi.org/10.3390/app132212385>

Academic Editor: Fausto Famà

Received: 8 October 2023

Revised: 8 November 2023

Accepted: 12 November 2023

Published: 16 November 2023



Copyright: © 2023 by the authors. Licensee MDPI, Basel, Switzerland. This article is an open access article distributed under the terms and conditions of the Creative Commons Attribution (CC BY) license (<https://creativecommons.org/licenses/by/4.0/>).

1. Introduction

Retrograde intrarenal surgery (RIRS) is a standard procedure dedicated to the treatment of kidney stones. The continuous development of endourology allows the use of minimally invasive treatment methods that improve patient safety. In the case of RIRS, regardless of the necessary armamentarium used for the procedure, the most crucial aspect is the balance of physical conditions (intrarenal pressure and temperature) prevailing in the operated space, the pelvicalyceal system of the kidney. Until now, there has been no standardised and universally available method to assess physical conditions in the renal pelvis in real time during flexible ureterorenoscopy [1], hence the need for experimental research to improve endourological techniques, which will lead to more effective surgery and better patient safety. The predominant conditions in the renal pelvis during RIRS are the result of several factors that influence the outcome of laser lithotripsy under optimal visibility conditions. The most important factor includes the balance between irrigation inflow (the IPP-generating irrigation system) and outflow (ureteroscope: ureteral access sheath ratio) [2–4].

The normal ('physiological') intrarenal pressure range is 0–20 cmH₂O [2]. Intrarenal backflow (flow from the renal pelvis to the renal parenchyma) and impaired arterial

perfusion have been reported at approximately 40 cmH₂O in both human [3] and animal studies [4]. Pressure above 40 cmH₂O leads to a pyelovenous backflow [5]. Previously published studies have shown that during flexible ureterorenoscopy, a very high peak IPP of up to 300–400 cmH₂O can be generated [6,7]. Therefore, the use of UAS (ureteral access sheath) during RIRS is one of the ways to reduce IPP. The application of UAS allows the safe insertion of endoscopic tools into the upper urinary tract and their easier navigation, as well as the improvement of vision by continuous flow establishment. Based on the cadaver study performed by Rehman et al., application of UAS during surgery results in an increase in irrigation flow of 35 to 80% compared to the group without the UAS used [8]. Irrigation pressures transmitted to the renal pelvis are significantly higher during flexible URS without the use of the UAS. Auge et al. showed that, regardless of the type of ureteroscope or the position of the UAS, the irrigation pressures transmitted to the renal pelvis are significantly greater during flexible URS with no utility of the UAS (pressure measured in the renal pelvis through the nephrostomy tube without the use of UAS was more than twice as high compared to measurements with UAS) [9].

The aim of the study was to evaluate IPP during RIRS procedures on 3D printed models with chemically synthesised stones. The 3D model allows RIRS procedures to be carried out under almost identical conditions, using stones of comparable size and density. The study evaluated the differences in real-time IPP generated during RIRS with two different sizes of UAS (10/12Fr vs. 12/14Fr) using different energy settings generated by the holmium:YAG laser. To the best of our knowledge, this is the first study to assess IPP in ex vivo conditions using 3D models created from plasticised thermoplastic polyurethane with chemically synthesised stones.

2. Materials and Methods

2.1. The 3D Printed Renal Pelvicalyceal Model and Stone Development

On the basis of the computed tomography (CT) scans, DICOM files were extracted, and the model was created. The first essential task was to determine the structure of the model in order to select the appropriate method, and then transform it morphologically using Boolean operations, followed by the creation of a “triangle network” mask with specified parameters and density, and then exporting the 3D image to an a.stl file (Figure 1a). The pelvicalyceal tract model was obtained using the Ultimaker 2+ Connect 3D printer working in Fused Filament Fabrication (FFF) technology, from plasticised thermoplastic polyurethane (TPU) according to patent application P.442625 (application to the Patent Office of the Republic of Poland on 24 October 2022—WIPO ST 10/C PL442625). The phosphate stones were chemically synthesised from phosphate salts (calcium phosphate), which were mixed in a 3:1 ratio with distilled water and acrylic styrene resin (1:1) (Figure 1b). A hydraulic press at a pressure of 3 MPa was used. The roasting temperature in the tube furnace was 950 °C.

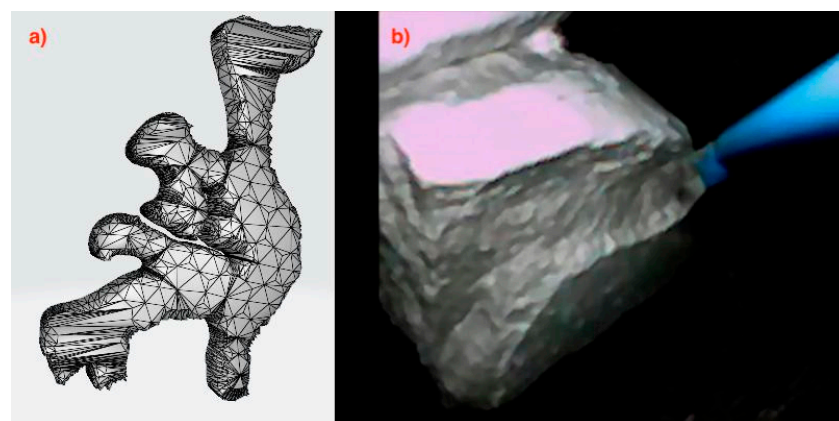


Figure 1. The stl. file of the 3D image of pelvicalyceal system (a). Intraoperative view of the artificial stone placed in the renal pelvis model during the procedure (b).

2.2. Intrapelvic Pressure Measurement

IPP monitoring during RIRS was performed using PressureWire X Guidewire (Abbott Medical, Plymouth, MA, USA) compatible with the CoroFlow system (Coroventis Research AB, Uppsala, Sweden) dedicated to displaying measured values. The pressure measurement method used in the study is one of the tools available for real-time pressure measurement in the renal pelvis. The PressureWire Guidewire has been used in two studies published hitherto. Doizi et al. analysed pressure measurements during five flexible ureterorenoscopies for kidney stone disease [6]. In the prospective pilot study by Sierra et al., the system was used during flexible ureterorenoscopy for different treatments (authors included 20 patients in the study) [10]. The pressure signal was transmitted wirelessly to the CoroFlow system using a CoroHub transmitter (Figure 2). The sampling rate of the CoroFlow system reaches 100 Hz, and the accuracy of pressure measurement is 0.1 mmHg. The CoroFlow measures the pressure values automatically in mmHg; therefore, for the purposes of our study, the results obtained were converted to cmH₂O. The recordings of the IPP generated during the procedures were blinded to the operator and assistant.

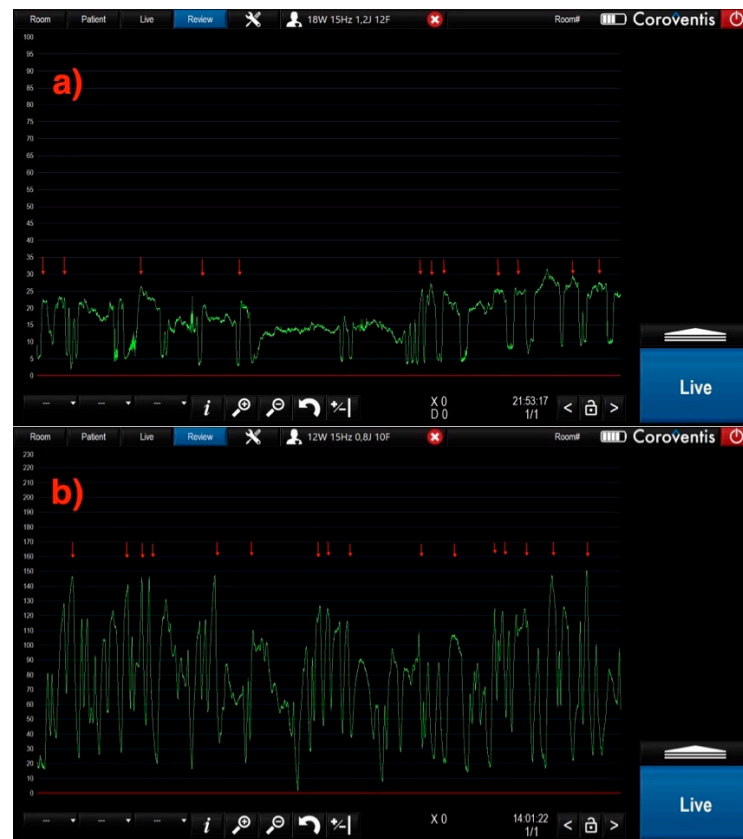


Figure 2. IPP recording during the procedure using 12/14Fr UAS (a), and 10/12Fr UAS (b). The pressure values seen in the graphs are given in mmHg. The red arrows indicate when the hand pumping system for irrigation was used. UAS—ureteral access sheath; IPP—intrapelvic pressure.

2.3. Study Design

The 3D printed model and the chemically synthesised stones were used in the study. All RIRS procedures were performed under almost identical conditions using a 3D model and phosphate artificial stones of comparable size deposited in the renal pelvis of the model. The 3D printed pelvicalyceal system, together with the ureteropelvic junction, was sealed with hot melt adhesive after placing the stone in the renal pelvis. The average stone size was 471.6 mm³ (the volume was calculated according to the formula of Sorokin et al. $A \times B \times C \times 0.524$ [11]). The average dimensions of the stones were as follows: length 15 mm, width 12 mm, height 5 mm. The mean stone density in NCCT was 1021 HU

(620–1383, SD \pm 150). A flexible ureteroscope (Pusen, Zhuhai, China; PU3022A) was used by insertion through the 10/12Fr (Flexor; Cook Medical; Bloomington, IN, USA) or 12/14Fr (ReTrace; Coloplast, Fontenay-sous-Bois, France) ureteral access sheath, which was placed approximately 1 cm below the model ureteropelvic junction. The ureteral access sheath was attached to the model with a rubber connector. A holmium:YAG laser (Quanta System Cyber Ho 60 W; Samarate, Italy) with a 272 mm laser fibre (Quanta System; Samarate, Italy) was used to fragment the stones (Figure 3).

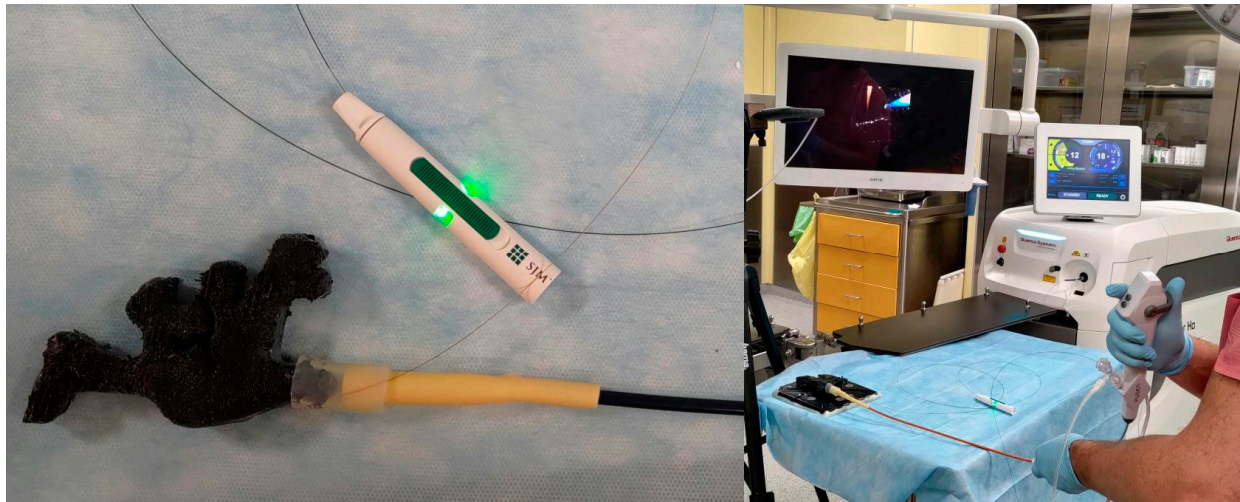


Figure 3. The 3D model of the pelvicalyceal system connected to the UAS with the PressureWire Guidewire. UAS—ureteral access sheath.

Constant gravity-based irrigation was used, with a height of 50 cm above the model, and a hand pumping system if necessary. The hand pumping system was used on-demand during lithotripsy when reduced visibility made it difficult to continue the procedure. The operator has 15 years of experience in endourology, including 8 years of experience in RIRS. The laser energy and pulse frequency were used in 7 fixed settings. The laser power ranged from 12 to 25 watts. The pulse frequency was in the range of 10 to 50 Hz, while the energy was in the range of 0.3 to 2.5 joules. All procedures were carried out in dusting mode using the virtual basket option. Endourological materials, such as flexible ureteroscope, holmium laser fibre, and ureteral access sheath, were recycled and disinfected for study use. The PressureWire was placed in the model's renal pelvis. We started recording intrapelvic pressure measurements after filling the model with fluid shortly before beginning the lithotripsy. The baseline intrapelvic pressure in the model after fluid filling was 6.8 cmH₂O.

2.4. Methodology

The significance level of the statistical tests in this analysis was set at $\alpha = 0.05$. The remaining pressure values with units of mmHg were multiplied stepwise by 1.35951 to convert to cmH₂O. The effects of the categorical explanatory variables *group* (two categories) and the *parameter* (seven categories) on the numerical IPP response variable were estimated using a multiple linear regression model.

The model was designed as a 7×2 factorial ANCOVA and fitted with the ordinary least squares (OLS) estimator based on Formula (1):

$$IPP_i = \beta_0 + \beta_1 \cdot group_i + \beta_2 \cdot parameter_i \times group_i + \epsilon_i, \quad (1)$$

where $\epsilon_i \sim N(0, \sigma^2)$

β_0 represents the model intercept, the expected IPP for the baseline group and parameter categories. β_1 represents the expected increase in IPP in the case of a category of *group* different from the baseline with the baseline *parameter* category. β_2 represents the interaction effect between the *parameter* and the *group* as moderator. Finally, the error ϵ_i

terms represent the deviations between actual and predicted IPP that are not explained by a linear trend. The variability of these deviations from the regression model is denoted by σ^2 . The interpretation of the magnitude of the coefficients of determination of the fitted model was based on Cohen's convention. The deviation of the values of the coefficients of the regression model from zero was tested with the *F*-test. The mean IPP at all factor levels was estimated using the marginal means. In the first step, estimated marginal means were performed for the main effect of the group, and in the next for the interaction effect of the parameters within the groups. The significance of the differences between the estimated marginal means was determined using marginal contrast analysis. The effect sizes of the marginal contrasts with the corresponding confidence intervals were calculated using the pairwise differences of the estimates, taking into account the uncertainty in both the estimated effects and the standard deviation of the population (Cohen's *d* effect size). Standardised parameters were obtained by fitting the model on a standardised version of the data set. A Wald *t*-distribution approximation was used to calculate 95% confidence intervals and *p*-values.

2.5. Statistical Environment

Analyses were conducted using the R Statistical language (version 4.1.1; R Core Team, 2021) on Windows 10 Pro 64 bit (build 19045), using packages *lme4* (version 1.1.27.1), *Matrix* (version 1.5.1), *effectsize* (version 0.8.3), *emmeans* (version 1.8.2), *interactions* (version 1.1.5), *sjPlot* (version 2.8.14), *performance* (version 0.10.4), *modelbased* (version 0.8.5), *report* (version 0.5.1.3), *psych* (version 2.1.6), *broom* (version 1.0.1), *readxl* (version 1.3.1) and *dplyr* (version 1.1.2).

3. Results

3.1. Characteristic of the Sample

The results of pressure measurements provided during a total of 50 RIRS procedures in 3D printed models with chemically synthesised stones (25 RIRS procedures with the use of 10/12Fr UAS and 25 with the use of 12/14Fr UAS) were eligible for the study. The sample of $N = 4,880,251$ IPP readings in the 10/12Fr AUS ($n_1 = 2,957,775$) and 12/14Fr UAS ($n_2 = 1,922,476$) groups was analysed for seven parameters. Each parameter represented an aggregate holmium:YAG laser setting of the watts/hertz/joule value.

The descriptive statistics of the IPP distributions for groups 10/12Fr and 12/14Fr UAS without breakdown of parameters are shown in Table 1.

Table 1. The descriptive statistics of the IPP distributions for groups 10/12Fr UAS and 12/14Fr UAS. *Mdn*—median; *Q1*—the first quartile (25%); *Q3*—the third quartile (75%).

Group	n	cmH ₂ O			
		<i>M</i> (<i>SD</i>)	<i>Mdn</i> (<i>Q1</i> , <i>Q3</i>)	<i>Min</i>	<i>Max</i>
10/12Fr	2,957,775	175.0 (83.4)	172.0 (114.0, 228.0)	6.8	461.7
12/14Fr	1,922,476	22.6 (10.9)	21.3 (13.9, 29.0)	6.8	106.5

The descriptive statistics of the IPP distributions for the 10/12Fr and 12/14Fr UAS groups by individual parameters can be found in Table 2.

Estimation of the group effect on the IPP value was first investigated in the framework of a mixed model with a random effect in the form of parameter categories (formula: $IPP \sim \text{group} + (1 | \text{parameter})$). However, the results of the values of the coefficients of determination $R^2_{\text{Conditional}} = 0.58$, $R^2_{\text{Marginal}} = 0.56$, and the very low value of $ICC = 0.04$ evidenced a lack of variance differences within each category of random intercepts, so the effect of the group was estimated based on the OLS model.

Table 2. Descriptive statistics of IPP distributions for the 10/12Fr and 12/14Fr UAS groups by individual parameters. *W*—watts, *Hz*—hertz, *J*—joule; *Mdn*—median; *Q1*—the first quartile (25%); *Q3*—the third quartile (75%).

Parameter, W/Hz/J	Group	<i>n</i>	<i>cmH₂O</i>			
			<i>M (SD)</i>	<i>Mdn (Q1, Q3)</i>	<i>Min</i>	<i>Max</i>
12/15/0.8	10/12Fr	497,026	157.1 (78.8)	151.0 (99.7, 208.0)	6.8	414.7
	12/14Fr	190,023	18.3 (7.6)	17.5(12.9, 22.8)	6.8	86.9
15/15/1.0	10/12Fr	266,082	133.3 (63.4)	134.9 (91.6, 175.2)	6.8	332.4
	12/14Fr	297,294	19.7 (7.15)	19.9 (14.0, 24.5)	6.8	60.4
15/50/0.3	10/12Fr	755,398	182.1 (73.0)	183.4 (136.2, 225.5)	6.8	411.9
	12/14Fr	234,420	24.0 (11.9)	24.1 (12.6, 32.2)	6.8	94.4
18/15/1.2	10/12Fr	396,417	188.0 (74.9)	193.2 (135.7, 242.0)	6.8	461.7
	12/14Fr	272,102	23.0 (9.5)	23.7 (14.8, 29.9)	6.8	87.7
18/30/0.6	10/12Fr	314,585	204.8 (97.5)	204.6 (125.9, 275.3)	6.8	415.5
	12/14Fr	351,461	22.6 (11.5)	20.7 (13.3, 29.9)	6.8	106.4
20/10/2.0	10/12Fr	400,407	167.1(77.3)	163.1 (108.1, 217.9)	6.8	414.8
	12/14Fr	339,951	23.8 (11.5)	22.7 (14.6, 31.00)	6.8	96.1
25/10/2.5	10/12Fr	327,860	181.6 (106.8)	168.7 (94.4, 253.1)	6.8	414.6
	12/14Fr	237,225	25.8 (13.8)	23.0 (15.1, 34.9)	6.8	96.0

3.2. Study of Group and Parameter Effects on IPP in the Form of an ANCOVA Model

We fitted a linear model to predict IPP with group and parameter (formula: $IPP \sim \text{group} + \text{parameter} * \text{group}$). The model explained a statistically significant and substantial proportion of variance ($R^2 = 0.59$, $F(13, 4880237) = 5.32 * 10^5$, $p < 0.001$, $R^2_{adj} = 0.59$).

The estimated marginal means for the groups only and for the parameters within the groups can be found in Tables 3 and 4.

Table 3. Estimated marginal means (EMMs) of IPP for the 10/12Fr and 12/14Fr UAS groups. *SE*—the standard error; *95% CI*—95% confidence interval.

Group	<i>IPP, cmH₂O</i>		
	<i>EMMs</i>	<i>SE</i>	<i>95% CI</i>
10/12Fr	173.43	0.04	[173.36, 173.51]
12/14Fr	22.46	0.05	[22.37, 22.55]

Table 4. EMMs between the 10/12Fr and 12/14Fr groups conditioned by the parameters. *EMMs*—Estimated marginal means; *SE*—the standard error; *95% CI*—95% confidence interval.

Parameter	Group	<i>IPP, cmH₂O</i>		
		<i>EMMs</i>	<i>SE</i>	<i>95% CI</i>
12 W 15 Hz 0.8 J	10F/12F	157.08	0.09	[156.91, 157.26]
	12/14Fr	18.33	0.15	[18.04, 18.61]
15 W 15 Hz 1.0 J	10/12Fr	133.34	0.12	[133.10, 133.59]
	12/14Fr	19.68	0.12	[19.46, 19.91]
15 W 50 Hz 0.3 J	10/12Fr	182.11	0.07	[181.97, 182.25]
	12/14Fr	23.98	0.13	[23.73, 24.24]
18 W 15 Hz 1.2 J	10/12Fr	187.95	0.10	[187.75, 188.15]
	12/14Fr	23.03	0.12	[22.79, 23.27]
18 W 30 Hz 0.6 J	10/12Fr	204.80	0.11	[204.57, 205.02]
	12/14Fr	22.60	0.11	[22.39, 22.81]
20 W 10 Hz 2.0 J	10/12Fr	167.11	0.10	[166.92, 167.31]
	12/14Fr	23.76	0.11	[23.54, 23.97]
25 W 10 Hz 2.5 J	10/12Fr	181.63	0.11	[181.42, 181.85]
	12/14Fr	25.82	0.13	[25.57, 26.08]

The estimated marginal contrast for the group (10/12Fr-12/14Fr) in Table 3 was 150.98 cmH₂O, 95% CI [150.86, 151.10], SE = 0.06, $p < 0.001$ with large effect size, $d = 2.37$, 95% CI [2.37, 2.38], SE < 0.01.

The results of the contrast analysis along with the effect sizes between the 10/12Fr and 12/14Fr w groups for each parameter are shown in Table 4.

See Figure 4 for a visualisation of the IPP means of conditional effects between groups and the parameter predictor based on the results of Table 4.

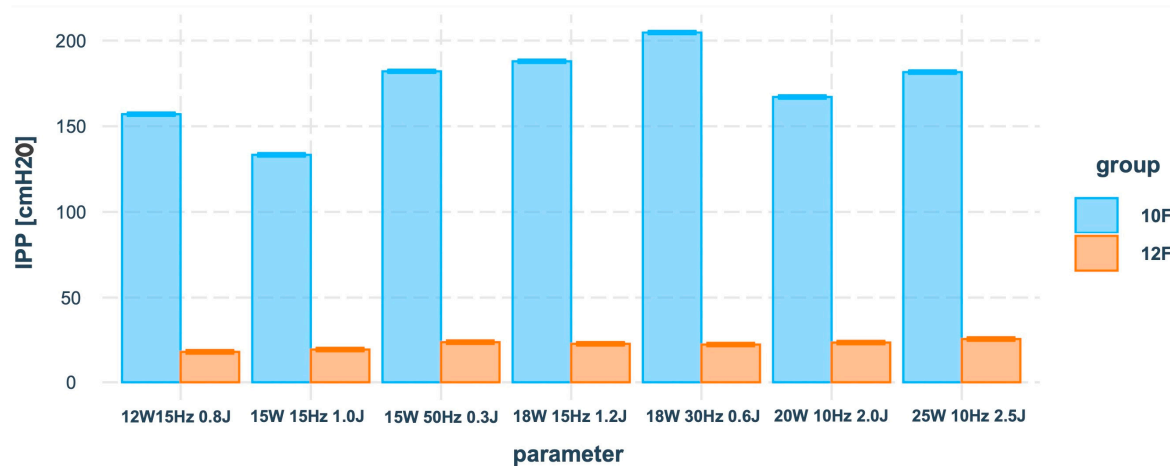


Figure 4. The IPP means of conditional effects between the categorical predictor *group* and the *parameter* based on the fitted regression model (the thick solid line at the top of the bars stands for 95% CI).

Calculation of the standardised model coefficients suggested that the absolute value of the main effect of the group factor on IPP $\beta_1 = |1.40|$ was much higher than the absolute values of the interaction effects of the parameter and the group factors $\beta_2 = [|0.10|, |0.48|]$.

The results of the contrast analysis in Table 5 showed significant differences between the 10/12Fr and 12/14Fr groups interpreted as large ($d \geq 0.80$).

Table 5. Results of contrast analysis with effect sizes between groups (10/12Fr-12/14Fr) for individual parameters. *p*—the *p*-value of the statistical test; *SE*—the standard error; *d*—Cohen’s *d* effect size; 95% CI—95% confidence interval.

Parameter	Contrasts				The Effect Size		
	Difference	95% CI	SE	<i>p</i>	<i>d</i>	SE	95% CI
12 W 15 Hz 0.8 J	138.76	[138.42, 139.09]	0.17	<0.001	2.18	<0.01	[2.18, 2.19]
15 W 15 Hz 1.0 J	113.66	[113.33, 113.99]	0.17	<0.001	1.79	<0.01	[1.78, 1.79]
15 W 50 Hz 0.3 J	158.13	[157.83, 158.42]	0.15	<0.001	2.49	<0.01	[2.48, 2.49]
18 W 15 Hz 1.2 J	164.92	[164.61, 165.64]	0.16	<0.001	2.59	<0.01	[2.59, 2.60]
18 W 30 Hz 0.6 J	182.19	[181.89, 182.50]	0.16	<0.001	2.86	<0.01	[2.86, 2.87]
20 W 10 Hz 2.0 J	143.36	[143.07, 143.65]	0.15	<0.001	2.25	<0.01	[2.25, 2.26]
25 W 10 Hz 2.5 J	155.81	[155.48, 156.15]	0.17	<0.001	2.45	<0.01	[2.44, 2.46]

4. Discussion

The enormous technological advances in endourology that have occurred over the past two decades of the 21st century have led to the dominance of minimally invasive methods in the catalogue of surgical treatments for kidney stones. The challenge of modern endoscopic urology in the treatment of urolithiasis is to establish a universally applied method for the real-time evaluation of physical conditions in the upper urinary tract during surgery. The consequences of increased IPP are urinary tract infections, increased risk of bleeding, and damage to the renal parenchyma [12,13]. Heretofore published studies

have indicated that, regardless of the IPP measurement method, the equipment used, or the instrument's size, the pelvic pressure generated can exceed the safe threshold value of 40 cmH₂O a few times. The morphological consequences for the kidney as a result of high IPP were revealed in animal studies. High pressure elicited diffuse denudation and flattening of the calyx urothelium, submucosal oedema and congestion, which were not observed in calyces undergoing low-pressure irrigation. Four to six weeks later, a higher incidence of columnar metaplasia, subepithelial nests, and periurethral vasculitis was observed in high-pressure treated calyces compared to low-pressure irrigated ones [14].

A factor with a protective function for the upper urinary tract during flexible URS is UAS. First applied in 1974 by Hisao Takayasu and Yoshio Aso [15], UAS is currently a standard option when performing flexible URS. Based on the results of the animal study reported by Neuraldin et al., a larger UAS (12/14Fr and 14/16Fr) mitigated intrarenal pressure, while smaller access sheaths (9.5/11.5Fr) provided inadequate drainage ureteroscopy [16]. Surgeons prefer a 10/12Fr and 12/14Fr size in most cases [1]; therefore, the primary objective of our study was to analyse the IPP according to these sizes of the UAS used. In addition, some studies have shown that a reduction in the size of the ureteroscope used for fixed-size UAS also results in a reduction in IPP [17–19].

The evidence on changes in IPP in the pyelocalyceal system during flexible URS is mainly based on single animal model studies published hitherto. Animal studies evaluated IPP using a wire inserted through a nephrostomy tube (in some studies, using urodynamic devices). The cutting-edge study was published in 2021 by Doizi et al. [6]. The authors, using a sensor (The PressureWire Guidewire) for real-time measurement of IPP inserted into the renal pelvis through the ureter, evaluated changes in intrapelvic pressure during flexible URS in four patients. Following the results reported by Doizi et al., the mean IPP during laser lithotripsy using on-demand forced irrigation was 115.3 cmH₂O. The maximum peak pressure measured during the therapeutic period using forced irrigation was 436 cmH₂O for UAS 10/12Fr, while for UAS 12/14Fr, it reached approximately 340 cmH₂O [6]. The second study that assessed IPP during flexible URS was one reported in 2023 by Sierra et al. Using PressureWire Guidewire, the authors measured changes in IPP in a group of 20 patients undergoing flexible URS. The median IPP during the therapeutic period with the use of forced irrigation on demand reached 61.2 (27.2–149.5) cmH₂O. The maximum peak pressure measured during the therapeutic period using forced irrigation was 236.6 cmH₂O for UAS 10/12Fr, while for UAS 12/14Fr, it reached 171 cmH₂O [10].

Printing a 3D model of the pelvicalyceal system on the basis of a RIRS trainer (according to the patent application P.442625) and producing chemically synthesised stones allowed a statistically significant series of RIRS procedures to be performed under almost the same conditions, as well as using PressureWire Guidewire to measure the dynamics of IPP (total of 50 procedures). For the first time, the authors used a 3D model that allowed simulation of the RIRS procedure to assess IPP. The study performed provides a new complement to the knowledge of IPP during flexible URS, and repeatable ex vivo conditions allowed RIRS to be simulated using different holmium laser parameters without any risk to the patient. For the printing of the model, thermoplastic polyurethane (TPU) was chosen after the available materials were analysed because, to the authors' knowledge, it most closely reflects the biostructure in terms of hardness and elasticity. In comparison, one of the new 3D models of the upper urinary tract dedicated to the simulation of the RIRS procedure is the model proposed by Orecchia et al. The authors introduced the models of the upper urinary tract which were digitally optimised and 3D printed from real-life cases. An additional advantage of the trainer is 3D printed models of urinary stones with two different degrees of hardness. The presented system allows us to perform RIRS simulation, which allows us to learn how to explore the pelvicalyceal system, as well as the performance of lithotripsy [20]. Our model similarly allows us to learn how to navigate a flexible ureteroscope in the pelvicalyceal system, while chemically synthesised stones of different densities enable us to perform laser lithotripsy even more faithfully, which, according to the perception of the surgeons participating in the testing phase of the trainer, practically

reflects the real lithotripsy in the patient's body. The lithotripsy of chemically synthesised calculi is not free from the phenomenon of residual lithotripsy formation and the dusty environment in which we work, which fully reflects natural conditions. Another system for RIRS simulation is the model presented by Trelles Guzmán et al. It is also based on a 3D printout of the upper urinary tract, which allows us to learn how to manoeuvre flex-URS and how to mobilise and evacuate natural kidney stones deposited in the pelvicalyceal system using an endoscopic basket. The model in the presented version does not allow one to simulate laser lithotripsy [21].

According to our study, the median IPP measured during the therapeutic period using forced irrigation on demand was 172 cmH₂O for UAS 10/12 Fr, while for UAS 12/14Fr, it was 21 cmH₂O. The maximum peak pressure measured during the therapeutic period using forced irrigation on demand was 461.7 cmH₂O for UAS 10/12 Fr, while for UAS 12/14Fr, it reached 106.5 cmH₂O. The estimated marginal means (EMMs) of IPP for the 10/12Fr and 12/14Fr groups were 173.43 cmH₂O and 22.46 cmH₂O, respectively. The results of the contrast analysis showed significant differences between the 10/12Fr and 12/14Fr groups regardless of the laser parameters used. The size of the UAS is an important determinant of the IPP generated during surgery that, with the current technology stage that does not allow for continuous intraoperative pressure monitoring, is an important element that the surgeon should always consider.

The use of the PressureWire Guidewire with retrograde approach provides an effective and safe tool for monitoring IPP, a system that is dedicated to assessing the pressure gradient in the coronary arteries, while in endourology it is currently being used in an experimental phase. At the experimental stage, a preliminary assessment of the system used could already be made: the 0.36 mm wire is safe for the patient, and it allows real-time measurement of IPP; the guidewire works in wireless mode, which greatly facilitates work during RIRS. A notable drawback is the high price and the single use option. In addition, performing lithotripsy during RIRS with PressureWire Guidewire in the pelvicalyceal system requires the operator to take additional care with the laser fibre especially when the working space in the kidney is small (in our study, wire damage occurred during a single procedure due to the laser beam being directed on the wire). An innovation in endourology equipment is the LithoVue Elite (LVE) ureteroscope (Boston Scientific Corp., Marlborough, MA, USA), the first flexible ureterorenoscope with the capability of continuous intraoperative monitoring of IPP during RIRS. In September 2023, the first results of the study using the new system were published. Bhojani et al. reported the results of a single-arm retrospective observational analysis of 50 patients undergoing RIRS. The authors conclude that the new ureteroscope will allow us to better understand the role that IPP plays in the clinical outcomes of URS [22].

Study Limitations

The experimental study highlights the importance of IPP evaluation during laser lithotripsy; however, it is not devoid of some limitations. The idea of the study was to evaluate the effect of the size of the UAS used on the IPP during laser lithotripsy, and hence, the study was designed to maximise the similarity of the lithotripsy conditions, with the variables being the size of the UAS and the holmium laser parameters. Three-dimensional printed models based on CT images of a patient were used for the study. The thermoplastic polyurethane used to print the models does not replicate the natural elasticity of the pelvicalyceal system; however, according to experts in the field, it matches the physical parameters of the renal collecting system. The models were printed according to the patent application but were not externally validated. The chemically synthesised stones were placed only in the renal pelvis of the models to standardise the conditions in the working space of the renal collecting system.

5. Conclusions

The use of UAS during RIRS is an essential factor in reducing the risk of high IPP generation, which is particularly crucial when we still do not have the capability to continuously monitor pressure during the procedure in daily surgery. The results of the contrast analysis of our study on 3D printed models showed significant differences between the 10/12Fr and 12/14Fr UAS groups regardless of the laser parameters used. The study confirmed that a high IPP of up to 400 cmH₂O would be achieved during f-URS with a handheld irrigation device using a 10/12Fr AUS, while the use of a 12/14Fr AUS would significantly reduce the peak pressure to approximately 100 cmH₂O. Obviously, our ex vivo results cannot be extrapolated directly to the operating room, but they constitute a new step in understanding the mechanisms of physical changes that occur in the upper urinary tract during flexible ureterorenoscopy.

Author Contributions: Conceptualization, K.B.; Methodology, K.B. and M.O.; Resources, A.P.; Writing—original draft, K.B. and A.P.; Supervision, M.O. All authors have read and agreed to the published version of the manuscript.

Funding: This research received no external funding.

Institutional Review Board Statement: Not applicable.

Informed Consent Statement: Informed consent was obtained from all subjects involved in the study.

Data Availability Statement: All the data are available within the study.

Acknowledgments: Many thanks to Celina Swiecinska for her outstanding support for the study.

Conflicts of Interest: The authors declare no conflict of interest.

References

1. Tokas, T.; Tzanaki, E.; Nagele, U.; Somani, B.K. Role of Intrarenal Pressure in Modern Day Endourology (Mini-PCNL and Flexible URS): A Systematic Review of Literature. *Curr. Urol. Rep.* **2021**, *22*, 52. [\[CrossRef\]](#) [\[PubMed\]](#)
2. Jung, H.; Osther, P.J.S. Intraluminal pressure profiles during flexible ureterorenoscopy. *Springerplus* **2015**, *4*, 373. [\[CrossRef\]](#) [\[PubMed\]](#)
3. Boccafroschi, C.; Lugnani, F. Intra-renal reflux. *Urol. Res.* **1985**, *13*, 253–258. [\[CrossRef\]](#)
4. Thomsen, H.S.; Dorph, S.; Larsen, S.; Talner, L.B. Intrarenal backflow and renal perfusion during increased intrapelvic pressure in excised porcine kidneys. *Acta Radiol. Diagn.* **1983**, *24*, 327–336. [\[CrossRef\]](#) [\[PubMed\]](#)
5. Pauchard, F.; Ventimiglia, E.; Corrales, M.; Traxer, O. A Practical Guide for Intra-Renal Temperature and Pressure Management during Rirs: What Is the Evidence Telling Us. *J. Clin. Med.* **2022**, *11*, 3429. [\[CrossRef\]](#)
6. Doizi, S.; Letendre, J.; Cloutier, J.; Ploumidis, A.; Traxer, O. Continuous monitoring of intrapelvic pressure during flexible ureteroscopy using a sensor wire: A pilot study. *World J. Urol.* **2020**, *39*, 555–561. [\[CrossRef\]](#)
7. Croghan, S.M.; Skolarikos, A.; Jack, G.S.; Manecksha, R.P.; Walsh, M.T.; O'Brien, F.J.; Davis, N.F. Upper urinary tract pressures in endourology: A systematic review of range, variables and implications. *BJU Int.* **2022**, *131*, 267–279. [\[CrossRef\]](#)
8. Rehman, J.; Monga, M.; Landman, J.; Lee, D.I.; Felfela, T.; Conradie, M.C.; Srinivas, R.; Sundaram, C.P.; Clayman, R.V. Characterization of intrapelvic pressure during ureteropyeloscopy with ureteral access sheaths. *Urology* **2003**, *61*, 713–718. [\[CrossRef\]](#)
9. Auge, B.K.; Pietrow, P.K.; Lallas, C.D.; Raj, G.V.; Santa-Cruz, R.W.; Preminger, G.M. Ureteral access sheath provides protection against elevated renal pressures during routine flexible ureteroscopic stone manipulation. *J. Endourol.* **2004**, *18*, 33–36. [\[CrossRef\]](#)
10. Sierra, A.; Corrales, M.; Kolvatzis, M.; Doizi, S.; Traxer, O. Real Time Intrarenal Pressure Control during Flexible Ureterorenoscopy Using a Vascular PressureWire: Pilot Study. *J. Clin. Med.* **2022**, *12*, 147. [\[CrossRef\]](#)
11. Sorokin, I.; Cardona-Grau, D.K.; Rehfuss, A.; Birney, A.; Stavrakis, C.; Leinwand, G.; Herr, A.; Feustel, P.J.; White, M.D. Stone volume is best predictor of operative time required in retrograde intrarenal surgery for renal calculi: Implications for surgical planning and quality improvement. *Urolithiasis* **2016**, *44*, 545–550. [\[CrossRef\]](#) [\[PubMed\]](#)
12. Tokas, T.; Herrmann, T.R.W.; Skolarikos, A.; Nagele, U.; Training and Research in Urological Surgery and Technology (T.R.U.S.T.)-Group. Pressure matters: Intrarenal pressures during normal and pathological conditions, and impact of increased values to renal physiology. *World J. Urol.* **2018**, *37*, 125–131. [\[CrossRef\]](#) [\[PubMed\]](#)
13. Osther, P.J.S. Risks of flexible ureterorenoscopy: Pathophysiology and prevention. *Urolithiasis* **2017**, *46*, 59–67. [\[CrossRef\]](#)
14. Schwalb, D.M.; Eshghi, M.; Ian, M.D.; Franco, I. Morphological and physiological changes in the urinary tract associated with ureteral dilation and ureteropyeloscopy: An experimental study. *J. Urol.* **1993**, *149*, 1576–1585. [\[CrossRef\]](#)
15. Takayasu, H.; Aso, Y. Recent development for pyeloureteroscopy: Guide tube method for its introduction into the ureter. *J. Urol.* **1974**, *112*, 176–178. [\[CrossRef\]](#)

16. Noureldin, Y.A.; Kallidonis, P.; Ntsiotis, P.; Adamou, C.; Zazas, E.; Liatsikos, E.N. The Effect of Irrigation Power and Ureteral Access Sheath Diameter on the Maximal Intra-Pelvic Pressure During Ureteroscopy: In Vivo Experimental Study in a Live Anesthetized Pig. *J. Endourol.* **2019**, *33*, 725–729. [[CrossRef](#)] [[PubMed](#)]
17. Monga, M.; Bodie, J.; Ercole, B. Is there a role for small-diameter ureteral access sheaths? Impact on irrigant flow and intrapelvic pressures. *Urology* **2004**, *64*, 439–441; discussion 441–442. [[CrossRef](#)]
18. Fang, L.; Xie, G.; Zheng, Z.; Liu, W.; Zhu, J.; Huang, T.; Lu, Y.; Cheng, Y. The Effect of Ratio of Endoscope-Sheath Diameter on Intrapelvic Pressure During Flexible Ureteroscopic Lasertripsy. *J. Endourol.* **2019**, *33*, 132–139. [[CrossRef](#)]
19. MacCraith, E.; Yap, L.C.; Elamin, M.; Patterson, K.; Brady, C.M.; Hennessey, D.B. Evaluation of the Impact of Ureteroscope, Access Sheath, and Irrigation System Selection on Intrarenal Pressures in a Porcine Kidney Model. *J. Endourol.* **2021**, *35*, 512–517. [[CrossRef](#)]
20. Orecchia, L.; Manfrin, D.; Germani, S.; Del Fabbro, D.; Asimakopoulos, A.D.; Agrò, E.F.; Miano, R. Introducing 3D printed models of the upper urinary tract for high-fidelity simulation of retrograde intrarenal surgery. *3D Print. Med.* **2021**, *7*, 15. [[CrossRef](#)]
21. Trelles Guzmán, C.R.; Mainez Rodríguez, J.A.; Aguado-Maestro, I.; Cansino Alcaide, R.; Pérez-Carral, J.R.; Martínez-Piñeiro, L. 3D printed model for flexible ureteroscopy training, a low-cost option for surgical training. *Actas Urol. Esp. (Engl. Ed.)* **2022**, *46*, 16–21. [[CrossRef](#)] [[PubMed](#)]
22. Bhojani, N.; Koo, K.C.; Bensaadi, K.; Halawani, A.; Wong, V.K.; Chew, B.H. Retrospective first-in-human use of the LithoVue™ Elite ureteroscope to measure intrarenal pressure. *BJU Int.* **2023**. *online ahead of print*. [[CrossRef](#)] [[PubMed](#)]

Disclaimer/Publisher's Note: The statements, opinions and data contained in all publications are solely those of the individual author(s) and contributor(s) and not of MDPI and/or the editor(s). MDPI and/or the editor(s) disclaim responsibility for any injury to people or property resulting from any ideas, methods, instructions or products referred to in the content.